Published in final edited form as:
Nat Electron. 2020 March ; 3(3): 156–164. doi:10.1038/s41928-020-0382-3.

Bidirectional optical signal transmission between two identical devices using perovskite diodes

Chunxiong Bao[#1,2], **Weidong Xu**[#1,3], **Jie Yang**[#1,2], **Sai Bai**[1], **Pengpeng Teng**[1,4], **Ying Yang**[4], **Jianpu Wang**[3], **Ni Zhao**[5], **Wenjing Zhang**[2,*], **Wei Huang**[3,6,*], **Feng Gao**[1,*]

[1]Department of Physics, Chemistry and Biology (IFM), Linköping University, Linköping 58183, Sweden

[2]International Collaborative Laboratory of 2D Materials for Optoelectronics Science and Technology, Institute of Microscale Optoelectronics, Shenzhen University, Shenzhen 518060, China

[3]Key Laboratory of Flexible Electronics (KLOFE) and Institute of Advanced Materials (IAM), Jiangsu National Synergetic Innovation Center for Advanced Materials (SICAM), Nanjing Tech University (NanjingTech), 30 South Puzhu Road, Nanjing 211816, China

[4]State Key Laboratory of Mechanics and Control of Mechanical Structures, Nanjing University of Aeronautics and Astronautics, Nanjing 210016, China

[5]Department of Electronic Engineering, The Chinese University of Hong Kong, New Territories, Hong Kong SAR, China

[6]Shaanxi Institute of Flexible Electronics (SIFE), Northwestern Polytechnical University (NPU), 127 West Youyi Road, Xi'an 710072, China

[#] These authors contributed equally to this work.

Abstract

The integration of optical signal generation and reception into one device – and thus allowing bidirectional optical signal transmission between two identical devices – is of value in the development of miniaturized and integrated optoelectronic devices. However, conventional solution-processable semiconductors have intrinsic material and design limitations that prevent

[*]Correspondence to: wjzhang@szu.edu.cn (W. Zhang), iamwhuang@nwpu.edu.cn (W. Huang), feng.gao@liu.se (F. Gao).

Data availability

The data that support the plots within this paper and other findings of this study are available from the corresponding author upon reasonable request.

Author contributions

F.G. and C.B. conceived the idea; W.X. and P.T. fabricated the perovskite devices and performed the electroluminescence (EL) efficiency characterizations; C. B. and J.Y. performed the EL speed and photodetection measurements and the application demonstrations; S.B. synthesized and tailored the ZnO nano-crystal and contributed to improve the device performance; F.G., W.H. and W.Z. guided the experiments and discussed the data; F.G., C.B., W.X., J.Y. and S.B. wrote and revised the manuscript, J.W., N.Z. and Y.Y. contributed to the result analysis and the revision of the manuscript; F.G. supervised the project; All authors discussed the results and commented on the manuscript.

Competing interests

The authors declare no competing interests.

Europe PMC Funders Author Manuscripts

Europe PMC Funders Author Manuscripts

them from being used to create such devices with high performance. Here, we report an efficient solution-processed perovskite diode that is capable of working in both emission and detection modes. The device can be switched between modes by changing the bias direction, and it exhibits light emission with an external quantum efficiency of over 21% and a light detection limit on a sub-picowatt scale. The operation speed for both functions can reach tens of megahertz. Benefiting from the small Stokes shift of perovskites, our diodes exhibit high specific detectivity (more than 2×10^{12} Jones) at its peak emission (~804 nm), allowing optical signal exchange between two identical diodes. To illustrate the potential of the dual-functional diode, we show that it can be used to create a monolithic pulse sensor and a bidirectional optical communication system.

Bidirectional optical signal transmission typically requires two sets of optical transmitters and receivers. However, integrating the functionalities of transmitter and receiver into one device, and creating bidirectional optical signal transmission between two identical devices, is important for miniaturized and monolithic optoelectronic systems[1,2]. Such dual-functional devices have previously been fabricated with III–V semiconductors[1,2], but their creation using solution-processed semiconductors is of particular interest due to their lightweight, mechanical flexibility, and simple integration with complementary metal–oxide–semiconductor (CMOS) technology[3–7].

Creating devices with satisfactory performance using solution-processable semiconductors (such as organic semiconductors or colloidal quantum dots) is though challenging due to intrinsic limitations in material properties and device structures. Specifically, the large Stokes shift of organic semiconductors make it impossible for organic light-emitting diodes (LEDs) to effectively absorb the light emitted by an identical device[8,9]; the bulk heterojunction (BHJ) structure of organic photodetectors is also not suitable for light emission because of the luminescence quenching in the BHJ layer[10]. For quantum dot LEDs, their thin recombination zone (1 to 2 monolayers) and poor charge transport limit the thickness of the emitting layer[11,12], making it far thinner than the optimal thickness required for photodetectors and limiting the detection sensitivity[13–15].

Metal halide perovskites are versatile and solution-processable semiconductors that have shown strong performance for both light emission and detection[16–31]. For example, perovskite LEDs have demonstrated external quantum efficiencies (EQEs) above 20% (ref. 25–29), and perovskite photodetectors have achieved a low detection limit of sub-pW cm^{-2}, as well as nanosecond scale response times[20–22]. These advances, together with the small Stokes shift of perovskite materials[32], suggest that high performance solution-processable dual-functional perovskite diodes, which can simultaneously function as an optical transmitter and receiver for bidirectional optical communications, could be developed. But efforts to create such dual-functional perovskite devices has so far had limited success.

Most high-efficiency perovskite emitters are based on quasi-two-dimensional structures, consisting of different thickness of PbI_6 sheets sandwiched by bulky cations[33]. A cascade energy transfer from the large-gap component to the small-gap component is observed and hence the emission occurs at the band tail close to that of three-dimensional (3D) perovskites[24,34]. In addition to enhancing the radiative recombination rate, this concept minimizes optical losses from reabsorption due to reduced absorption–emission spectral

overlap[24,26,34,35]. This is clearly favourable for LED performance, but makes the device insensitive to detecting light emitted by the identical devices. Furthermore, the response time for perovskite LEDs have rarely been investigated, but such measurements are important for dual-functional devices and their application in optical communications. In addition, the common device structure for perovskite photodetectors is not applicable for efficient light emission due to the strong photoluminescence (PL) quenching induced by the charge transport layers[20–22].

In this Article, we report optical signal transmission between two identical dual-functional diodes based on high-efficiency 3D perovskite emitters. The large absorption emission spectral overlap of 3D perovskite emitters provides the opportunity for solution-processed semiconductors to achieve high sensitivity to the light emitted from the identical device. The perovskite diodes demonstrate efficient and intense light emission with an EQE over 21% under the positive bias, and a high sensitivity reaching the sub-picowatt scale when operating as photodetectors under zero or reverse bias. We also show that a fast response speed reaching tens of megahertz (MHz) can be obtained as both light emission and detection devices, making them promising for optical communication. With this approach, we build an efficient bidirectional optical communication system based on two identical perovskite diodes (Fig. 1a) and a photoplethysmogram sensor for arterial pulse wave tracking.

Perovskite diode as a light-emitting device

The device structure of the perovskite diodes is indium tin oxide (ITO)-coated glass/ polyethylenimine ethoxylated (PEIE)-modified zinc oxide (ZnO)/formamidinium lead iodide ($FAPbI_3$) perovskite (~50 nm)/poly(9,9-dioctyl-fluorene-co-N-(4butylphenyl)diphenylamine) (TFB; ~40 nm)/molybdenum oxide (MoO_x; ~7 nm)/gold (Au; ~80 nm) (Fig. 1a). An efficient passivation agent of 2,2′-[oxybis(ethylenoxy)]diethylamine (ODEA) developed in our recent work[29] is used to minimize the defects in the perovskite layer. As we show in Fig. 1b, when the diode works under a positive bias larger than the turn-on voltage, the electrons and holes are injected into the perovskite emitters and generate light emission via efficient radiative recombination. Similarly, when the diode works under a zero or reverse bias, upon excitations by photons with energy equal to or higher than the bandgap of the perovskite, the photo-generated carriers are separated and collected as an electrical signal (Fig. 1b). The optimized perovskite diode (with 30% ODEA passivation and precursor concentration of 0.13 M) simultaneously show optimal electroluminescence (EL) (Supplementary Fig.1) and photodetector performance (as discussed later). The absorption and PL spectra of the optimized perovskite film in Fig. 1c show a large overlap with only a small Stokes shift (~40 meV), indicating that the perovskite film would be sensitive to the light emitted by the same film.

We first demonstrate the high performance and fast response speed of the perovskite diodes as LEDs. The characterization results show a low turn-on voltage of ~1.3 V (Supplementary Fig. 1a) and a maximum radiance of ~314 W sr^{-1} m^{-2} (Fig. 2a). A peak EQE of 21.2% is obtained, which is among the highest reported EQE values of perovskite LEDs[25–29]. The

high EL performance of our devices mainly benefits from the effective passivation of ODEA to the iodide vacancy on the perovskite crystal surfaces, which have been investigated in details in our previous work[29].

For the characterization of the response speed, we first monitor the evolution of the EL intensity and current of the diodes driven by square-wave voltages (Fig. 2b). At a low frequency of 100 Hz, both the EL intensity and the current well follow the change of the drive voltage. In the case of higher frequency of 100 kHz, we observe a slight lag of the EL intensity to the voltage change as well as obvious overshoots of the current, which may result from the charging and discharging effects of the parasitic capacitance. In order to confirm it, we fit the transient current curves with an exponential function and obtain time constants of ~120 ns and ~172 ns for the charging and discharging processes, respectively (Supplementary Fig. 2a). Considering a serially connected resistance (50 Ω) to the device, the device capacitance is determined to be 2.9±0.5 nF. This calculated value agrees well with the measured value (Supplementary Fig. 2b), indicating that the parasitic capacitance of the device limits the response speed when functioning as an LED. We note that passivation of trap states can not only boost the EL efficiency but also reduce the parasitic capacitance (Supplementary Fig. 2b) and consequently improve the response speed (Supplementary Fig. 2c). We further measure the EL frequency response of the perovskite diode driven by different voltages to determine the cutoff frequency of the device. As shown in Fig. 2c, the cutoff frequency increases with increasing drive voltage and shows a maximum 3-dB cutoff frequency of 1.90 MHz at 4.0 V. The increase of the cutoff frequency can be attributed to faster injection of charges under higher drive voltage, similar to that observed in inorganic and organic diodes[36–38].

Since the parasitic capacitance is affected by the device area, we further study the device-area-dependent speed of the perovskite LEDs. We show 3-dB cutoff frequencies of the LED with different device areas in Fig. 2d, which demonstrates an increased 3-dB cutoff frequency with decreasing device area, from 1.9 MHz for 7.25 mm^2 device to 21.5 MHz for 0.1 mm^2 device. Considering its relatively large area, our device is among the fastest solution-processed LEDs[38,39]. The nearly linear increase of the cutoff frequency with decreasing device area (Supplementary Fig. 2d) origins from the smaller parasitic capacitance of the device with a smaller active area, indicating that the response speed of our devices is dominated by the resistance-capacitance (RC) constant. Therefore, a further improvement of the response speed can be expected by reducing the device area.

Perovskite diode as a photodetector

Having demonstrated efficient and fast response of our devices when functioning as LEDs, we proceed to investigate the device performance when working as photodetectors. We notice that the ODEA passivation can significantly reduce the dark current (Supplementary Fig. 3a) and measure a low dark current of 0.3 nA at -1 V with the optimized ODEA passivation, as shown in the current density-voltage (J-V) curves in Fig. 3a. The photon-to-current EQE spectra of our diodes (Supplementary Fig. 3b) exhibit a wide photoresponse range from ultraviolet (UV) to near infrared (NIR) region (350 to 800 nm). The EQE peak at around 380 nm can be attributed to the response of the hole transport layer TFB, which can

be evidenced by the excitation spectrum of TFB (Supplementary Fig. 3b). The EQE spectra of the devices fabricated from perovskite precursors with different concentrations (Supplementary Fig. 3c) show that the EQE reaches a maximum value when the precursor concentration is 0.13 M, which is also the optimized concentration for light-emitting devices. The photocurrent (Fig. 3a) and EQE values (Supplementary Fig. 3b) of the photodetector at visible to NIR region (400-800 nm) show only a marginal decrease under 0 V bias as compared to the reverse bias, implying low energy barriers at the interfaces between the perovskite layer and its neighboring charge transport layers. In order to provide further evidence, we simultaneously monitor the relative photon-to-current EQE and PL quantum efficiency (PLQE) of the device under different biases. As shown in Supplementary Fig. 4a, under 1 μW excitation (450 nm), the PLQE shows nearly a constant ~80% quenching under both 0 V and reverse bias compared with its peak value, and the EQE is nearly constant during the same bias range. This result indicates efficient charge separation and collection at 0 V bias, rationalizing the fact that the devices can work as efficient photodetectors.

To evaluate the lowest detectable limit of our perovskite diodes as photodetectors, we perform the dark current noise measurement and calculate the noise equivalent power (NEP). In Supplementary Fig. 4b, we show the dark current noise of the diodes under different bias voltages. We also calculate the shot noise and thermal noise based on the dark currents and the differential resistances (see Methods section). The calculated shot noise and thermal noise are from 2.4 to 9.1 fA $Hz^{-0.5}$and 1.2 to 5.4 fA $Hz^{-0.5}$ under -0.1 to -1.0 V bias, corresponding to a total noise from 2.7 to 10.7 fA $Hz^{-0.5}$. This value agrees well with the measured values in Supplementary Fig. 4b, indicating that the noise current is dominated by the shot noise and thermal noise. Based on the EQE spectra and the measured noise, we evaluate the NEP to be 1.6×10^{-14} W $Hz^{-0.5}$ (under 0 V bias, at 670 nm where the EQE reaches the peak value). We also experimentally perform the weak light response measurement and obtain a measured detectable light power of 0.8 pW for 630 nm red light (Supplementary Fig. 4c). Our devices show linear response from the lowest detectable limit (0.8 pW) to 20 μW, corresponding to a linear dynamic range of 148 dB (Supplementary Fig. 4d). We further calculate the specific detectivity (D*) spectra and show the results in Fig. 3b. We achieve a peak D* of 5.3×10^{12} Jones in the visible region, which is among the highest reported values for perovskite diodes[20–23]. Meanwhile, the photodetector shows high D* (2.0×10^{12} to 3.8×10^{12} Jones) at ~800 nm, indicating high sensitivity of the photodetector to the light emitted from the identical diode.

We further perform transient photocurrent (TPC) to investigate the response time of our diodes with different device areas (Fig. 3c). The device response time can be obtained by fitting the TPC curves with an exponential function. We observe a faster response time for a device with smaller active area, indicating that the parasitic capacitance also limits the response speed of the photodetector. This conclusion is further backed up by the observed constant response time under different reverse biases (Supplementary Fig. 5a), ruling out the possibility that the response time is limited by the transit time of the carriers and indicating the importance of the parasitic capacitance which affects the response time. The response time of the full-area (7.25 mm^2) device is fitted to be 237 ns (Fig. 3c), which is larger than the RC constant of the device measured under dark, due to a larger capacitance under

illumination (Supplementary Fig. 2b). When the active area is decreased to 0.1 mm^2, the pulse width (full width at half maximum, FWHM) of the TPC is ~6.8 ns and the falling time is ~3.9 ns (inset of Fig. 3c), which is among the fastest response times of perovskite photodetectors[20–23]. The fast response time of our perovskite photodetector also benefits from the effective passivation of the ODEA (Supplementary Fig. 5b, c). Based on the pulse width (Δt) of the TPC we obtain a bandwidth (f_{-3dB}) of the photodetector as ~65 MHz according to the relation $f_{-3dB}=0.44/\Delta t$. This bandwidth is close to that extracted from the frequency response curve obtained from the fast Fourier transform of the TPC curve (Supplementary Fig. 5d).

We also investigate the stability of the perovskite photodetector working at reverse bias under nitrogen atmosphere. The dark- and photo-current of the device under -0.5 V bias (Fig. 3d) show negligible changes during the entire test period (~42 hours), indicating excellent reliability and stability of the devices. It is worth mentioning that the stability of perovskite diodes under reverse bias is usually very poor due to the accumulation of ionic defects in the perovskite film under reverse bias[40]. We note that the efficient defect passivation of ODEA is critical for improving the device stability. The devices without ODEA passivation exhibit increasing and fluctuant dark currents under -0.5 V bias after several hours (Supplementary Fig. 6). Furthermore, our devices show stable EL spectrum after working as light emission and detection devices. As shown in Supplementary Fig. 7a, after working as the light emitting device at 25 mA cm^{-2} for a period of 20 hours, the peak position shows little change. Similarly, the EL peak position and intensity show negligible changes after working as the photodetector at -0.5 V bias for 10 hours (Supplementary Fig. 7b). It is worth noting that the stable device performance is obtained in a nitrogen environment inside a glovebox. Upon exposure to air, the device performance will significantly degrade in several minutes (Supplementary Fig. 8), suggesting the importance of developing encapsulation technologies for the perovskite devices in order to enable practical applications in the future.

Signal exchange between two perovskite diodes and demonstrations

To demonstrate the response of the perovskite diode to the light emitted from an identical diode, we study the opto-coupling performance between two identical perovskite diodes. Fig. 4a shows the photocurrent of perovskite photodetectors (under -0.5 V bias) responding to the light from an inter- or intra-chip perovskite LED driven by different current densities. The photographs of the inter- and intra-chip configurations are shown in the insets of Fig. 4b; the distance between the diodes for both intra- and inter-chip designs are ~1 mm (diode distance definitions are schematically shown in Supplementary Fig. 12a and Fig. 13a). The response waveforms of the perovskite photodetectors under 0 and -0.5 V bias to the emitted light from inter- and intra-chip LEDs are exhibited in Supplementary Fig. 9a-d. Fig. 4b shows the ratio of the photodetector (under -0.5 V bias) current to the LED drive current. For both inter-chip and intra-chip conditions, the current ratio increases with increasing drive current densities, because the light emission EQE increases with increasing drive current at low current region (Fig. 2a). Fig. 4c shows the frequency response between the photodetector and LED, indicating a 3-dB cutoff frequency of ~1.2 MHz, meaning that signals below 1.2 MHz can be well transmitted and received between our full-area (7.25

mm^2) perovskite dual-functional diodes. Supplementary Fig. 9e, f shows the measured 10 Hz and 1 MHz sinusoidal signals transmitted and received by our dual-functional diodes.

Dual-functional perovskite diodes as light emission and detection devices show great potentials in minimization and integration of optoelectronic devices or systems because the devices are based on the same structure and materials. To demonstrate their high sensitivity to the light emitted from the identical device and the ease of integration, we use monolithic perovskite diodes as the light source and sensor to build an optoelectronic heart pulse sensor. In this system, two perovskite diodes are fabricated on one chip. The light emitted from one diode propagates into the finger; part of the light is absorbed by the skin vascular bed, and the rest is transmitted though or reflected by the tissue and partially detected by the other diode (Fig. 5a). As the haemoglobin contained in blood can absorb a portion of the light, the volumetric changes of the blood flow due to the pumping of the heart will induce the change of the light absorption by the vascular bed, which can then be detected by the other diode. The photograph of the system is shown in Fig. 5b. The cardiac cycles measured with our dual-functional perovskite diodes agree well with those measured using a commercial pulse sensor, which includes an inorganic green LED and silicon photodiode (Fig. 5c). The exact waveforms obtained by these two sensors are similar. The slight difference is likely caused by the different penetration depth of the light as well as the difference in the signal acquisition circuits. The enlarged waveforms measured by the perovskite and commercial sensor shown in Fig. 5d can reflect the details of the pulse, including the systolic peak and diastolic notch[41,42]. In addition, the waveform of our perovskite devices is robust with time (Supplementary Fig. 10a) and reproducible in different devices (Supplementary Fig. 10b). The ease integration of two functionalities in one device not only greatly simplifies the design and process of devices, but also enables the miniaturization and even integration of different functionalized devices.

The fast response speed and high sensitivity to the light emission from the identical perovskite diode make these diodes promising for simplifying bidirectional optical communication systems. To demonstrate the feasibility of using them in a realistic optical communication system, we use two such perovskite diodes simultaneously as the transmitter and receiver to build a bidirectional optical communication system instead of conventional double transmitter/receiver systems (Fig. 5e). The data from a computer are modulated to the on/off status of the perovskite diode which works as the transmitter. The modulated light is then received by the other perovskite diode and transferred to the computer after amplification and demodulation. Through this system, we successfully realize bidirectional communication using two dual-functional perovskite diodes (Fig. 5f). The photograph and the video of the communication system are shown in Supplementary Fig. 11 and the attached video. Both analogue (Fig. 5g) and digital (Fig. 5h) signals can be transmitted and received by the perovskite dual-functional diodes. As shown in Fig. 5h and Supplementary Fig. 12, the digital signal can be exchanged between the full-area intra-chip dual-functional perovskite diodes (diode distance: 1 mm) at a bit rate of 1 Mbit/s. For inter-chip communication (diode distance: 13 mm), the bit rate is below ~100 kbit/s (Supplementary Fig. 13), which is mainly limited by the amplifier we use. Although the speed of the solution-processed perovskite device is expected to reach hundreds of MHz or even GHz (Supplementary Note 1), the values are still lower than those obtained in commercial devices

made from inorganic semiconductor devices. For example, III-V compound semiconductor laser diode[43] and LED[44] as transmitters have reached modulation speed of tens of GHz and 800 MHz, respectively; InGaAs p-i-n photodiodes as receivers have reached response speed faster than 100 GHz[45]. As such, the bandwidth of our current system is behind what is required for fiber-optic and visible light communication systems. However, we believe that our dual-functional perovskite diodes show great potential in middle and low speed (below tens of Mbit/s) optical communications, inter- and intra-chip data links for solution-processable optoelectronic integrated circuits.

Conclusions

We have shown that optical signal transmitter and receiver functions can be integrated in one device using metal halide perovskites. The two functions of the device can be reversibly switched by changing the bias direction. The diode shows high performance comparable to state-of-the-art single-function perovskite devices when working as either a light-emitting or light-detecting device. The response speed of the perovskite light-emitting device is systematically studied, and a high response speed of ~21 MHz demonstrated for a 0.1 mm^2 device. The perovskite diode shows high sensitivity to the light emitted by an identical diode, providing a unique opportunity to simplify the integration of optoelectronic devices. We demonstrate this through building a monolithic pulse sensor system and a bidirectional optical communication system based on two identical perovskite diodes. Furthermore, we expect that the response speeds of our devices could be further improved by decreasing the size of the pixel, since the devices are mainly limited by the parasitic capacitance. This would allow the development of high-speed display-to-display communication or data exchange. These features, coupled with the ease of integration on a wide range of inorganic substrates and compatibility with CMOS, make the dual-functional perovskite diodes promising for inter- or intra-chip data links in future solution-processed optoelectronic integrated circuits.

Methods

Device fabrication

Patterned ITO glass substrates (sheet resistance: ~10 ohm/sq, transmittance: ~88%) were firstly washed with detergent and then heated in ammonia and hydrogen peroxide mixed aqueous solution at 80 °C for 30 minutes, followed by UV-Ozone treatment for 20 minutes. ZnO nanoparticles dispersed in ethanol were spin-coated on the ITO substrates at 4000 rpm for 30 s in air to form a ZnO layer. After that, the ZnO-coated substrates were transferred to a nitrogen filled glovebox (H_2O level<0.1 ppm; O_2 level: 4.5-30 ppm). PEIE solution (0.05 wt% in isopropanol) was spin-coated on the ZnO layer at 5000 rpm for 30 s and then annealed at 100 °C on a hot plate for 10 minutes. Perovskite precursor solution in DMF (FAI:PbI_2:ODEA=2:1:0.3 in molar ratio, Pb^{2+} concentration: 0.13 M) was deposited on the ZnO/PEIE layer at 3000 rpm for 30 s and then annealed at 100 °C for 10 minutes. After cooling to room temperature, TFB (12 mg mL^{-1} in chlorobenzene) was spin coated on the perovskite film at 3000 rpm for 30 s, followed by the thermal evaporation deposition of 7 nm MoO_x (~0.5 Å/s) and 80 nm Au (~2 Å/s) at a pressure of 1×10^{-6} mbar.

Europe PMC Funders Author Manuscripts

Characterizations of materials and LEDs

Our perovskite films and devices were stored in nitrogen filled glovebox without being deliberately kept away from light. The thicknesses of the films were determined using a Bruker Dektak profilometer and the SEM cross-sectional images. The perovskite film deposited on ZnO/PEIE coated ITO substrate was used to perform the ultraviolet–visible (UV-vis) absorption spectra and PL spectra measurements. The UV-vis absorption spectrum was measured using a UV-vis spectrophotometer (Lambda 900, PerkinElmer) with a ZnO/PEIE coated ITO substrate as reference. The PL spectrum was measured using a spectrometer (Shamrock sr-303i-B, Andor Technology) and the exciting light was from a continuous wave laser (450 nm).

The performance of the LED was measured in a nitrogen filled glovebox. A Keithley 2400 source meter was used to power the device. The drive voltage was swept from 0 to 5 V with an interval of 0.02 V. At each voltage point, the EL spectra and intensities were monitored using a spectrometer (QE Pro, Ocean Optics) coupled with a fiber connected integrating sphere (FOIS-1). During the measurement, the devices were placed over the entrance aperture on the surface of the integrating sphere and only the forward emission light can be detected. To measure the transient current and EL characteristics of the LEDs, a square wave voltage with pulse voltage of 3.5 V was used to drive the LEDs. The current waveform was directly monitored by an oscilloscope with an input impedance of 50 Ω. The EL intensities were detected using a silicon photodiode (S1133, Hamamatsu) which was reversely biased (-9 V) with a 9 V lithium ion battery. The current signal of the silicon photodiode was monitored by the oscilloscope with an input impedance of 50 Ω. The transient current and EL measurements were carried out in air on an encapsulated LED. The frequency response and bandwidth of the LED were determined using unencapsulated devices in the nitrogen filled glovebox. The devices were driven by sinusoidal voltage and the average EL intensities were measured using the QE Pro spectrometer coupled with a fiber integration sphere. The frequency of the drive voltage was scanned from 1k to 50M Hz.

Photodetector characterizations

The characterizations of the photodetector were carried out in air at room temperature on encapsulated devices, unless otherwise specified. To encapsulate the devices, a drop of UV adhesive (~5 μL, Norland Products, NOA 73) is put on the metal electrode side of the device, then covered with a glass slide. After the adhesive fully permeates the space between the device and cover glass, it is solidified upon illumination with a UV lamp through the cover glass side for about 30 s. The J-V curves of the devices were measured using a Keithley 2400 source meter. The device was fixed in a grounded metal box. An aperture with a diameter of ~3 mm on the box allows the light to vertically shine on the device. For dark J-V curve measurements, the aperture was covered with a black tape. For photo J-V curve measurements, a 630 nm laser beam was used to illuminate the device. The diameter of the laser spot was about 1 mm and the power of the laser beam was adjusted by changing its drive current using a Keithley 2400 source meter and calibrated using a light power detector (Newport, 818-UV/DB).

The photo-to-current EQE of the device was measured using a solar cell spectral response measurement system (QE-R3011, Enli Technology) which was calibrated with a standard Si crystalline solar cell. The dark current noise spectra of the devices were measured using a lock-in amplifier (SR830, Stanford Research System) coupled with a low noise preamplifier (SR570, Stanford Research System). The sensitivity of the preamplifier was chosen to be 0.1 nA/V. The instrument noise was first measured without connecting the device to the input. The shot noise $i_{n,s}$, thermal noise $i_{n,t}$ and total white noise i_n were calculated based on the following equations:

$$i_{n,\,s} = \sqrt{2eI_D\,\Delta\,f} \tag{1}$$

$$i_{n,\,t} = \sqrt{\frac{4k_BT\,\Delta\,f}{R}} \tag{2}$$

$$i_n = \sqrt{i_{n,\,s}^2 + i_{n,\,t}^2} \tag{3}$$

where e the elementary charge, I_D the dark current, Δf the bandwidth, k_B the Boltzmann constant, T the temperature, R the resistance of the devices. With the EQE and dark current noise (i_n), the NEP and D^* of the device can be calculated based on the following equations:

$$NEP = \frac{i_n}{\mathscr{R}_\lambda} \tag{4}$$

$$D^* = \frac{\mathscr{R}_\lambda\sqrt{A}}{i_n} \tag{5}$$

$$\mathscr{R}_\lambda = \frac{I_{ph}}{P_{in}} = \frac{e\cdot\lambda\cdot EQE}{hc} \tag{6}$$

where $\mathscr{R}_\lambda$ is the responsivity of the device at wavelength λ, A the device area, I_{ph} the photocurrent of the devices when incident light power is P_{in}, h the Plank constant, and c the light speed.

To study the weak light response and LDR of the photodetector, a laser beam driven by a square wave voltage at a frequency of 8 Hz was used to illuminate the device. The output of the drive voltage kept alternating on/off at a period of 20 s. The light power was adjusted using neutral density filters and calibrated with the Si photodiode. The current signals of the devices were recorded by the lock-in amplifier. The LDR was calculated using the following equation:

$$\mathrm{LDR} = 20\lg\frac{P_{high}}{P_{low}} \tag{7}$$

Europe PMC Funders Author Manuscripts

where P_{high} and P_{low} are the highest and lowest light power among which the measured photocurrent of the devices shows linear relation with the incident light power.

The TPC of the photodetector was measured using the oscilloscope with an input impedance of 50 Ω when the device was excited by a pulse laser (wavelength: 337 nm, pulse width: ~4 ns) from a nitrogen laser (NL100, Stanford Research System) after attenuation with a neutral density filter. To measure the TPC of the device under reverse biases, a Keithley 2400 source meter was used to apply biases.

The stability of the photodetectors was investigated in the nitrogen filled glovebox on an unencapsulated device. The incident light was from a red LED (650 nm) which was driven by an alternating on/off voltage with a period of 20 s. The current of the photodetector was recorded by a Keithley 2400 source meter.

To study the current response of the perovskite photodetector to the light emitted from a perovskite LED with an identical structure, we used a Keithley 2400 source meter to drive the perovskite LED at various currents and the photocurrent of the photodetector was monitored using another source meter. To study the frequency response of the perovskite photodetector to light emitted from a perovskite LED with an identical structure, we used sinusoidal voltage with different frequency to drive the LED and used an oscilloscope to measure the current waveform of the photodetector.

Demonstration of the application

To demonstrate their application as the light source and detector in the biomedicine field, we used two identical diodes on one chip as the LED and photodetector for a heart pulse sensor. The LED was driven by a DC current of 2 mA from a source meter. One of the fingertips of C.X.B. was gently pressed on the device and simultaneously cover the LED and photodetector pixels. The current of the photodetector was monitored by an oscilloscope after amplification by a low noise current preamplifier with a 10-Hz lowpass filter (Fig. 5a, b). For comparation, a commercial pulse sensor integrated with a green inorganic LED, a silicon photodiode and filter/amplifier circuit were fixed on another finger and monitored by the oscilloscope simultaneously.

In the demonstration system of bidirectional optical communication, two identical diodes in the same or different chip was used as transmitter and receiver simultaneously. Two open-source electronics platforms (Arduino UNO) were used to convert digital data to high/low voltage level or vice versa. The user interfaces of the platforms allow the users to input and receive information on the computers. The information input by User1 was transferred to ASCII codes and then transmitted to the Arduino UNO board where the ASCII codes can be transferred to high/low voltage level on the specified pin. The voltage drove the perovskite LED and made it blink. The blinking light was then detected by the other perovskite diode, whose photocurrent was transferred to voltage through a current preamplifier and then input to the specified pin of the other Arduino UNO board, where the voltage signal was transferred to ASCII codes and transmitted to the computer. The computer then transferred the ASCII codes into words and displayed on the user interface for User 2. The information transmitted from User 2 to User 1 followed the same process. The audio signal was

transmitted as analogue signal. The signal was firstly amplified and used to drive one of the perovskite diodes through which the signal was modulated in the change of the on/off status. The light signal was received by the other perovskite diode and then amplified by a preamplifier before driving the loudspeaker.

Supplementary Material

Refer to Web version on PubMed Central for supplementary material.

Acknowledgements

We thank M. Kovalenko for helpful discussions. This work is supported by the ERC Starting Grant (Grant No. 717026), the Major Research Plan of the National Natural Science Foundation of China (Grant No. 91733302), the National Natural Science Foundation of China (Grant No. 51472164, 61704077), the National Science Fund for Distinguished Young Scholars (Grant No. 61725502), the 1000 Talents Program for Young Scientists of China, Shenzhen Peacock Plan (Grant No. KQTD2016053112042971), the Educational Commission of Guangdong Province (Grant No. 2015KGJHZ006), the Natural Science Foundation of Jiangsu Province (BK20171007), the European Commission Marie Skłodowska-Curie Actions (691210), the Swedish Government Strategic Research Area in Materials Science on Functional Materials at Linköping University (Faculty Grant SFO-Mat-LiU no. 2009-00971), the Nanjing University of Aeronautics and Astronautics PhD short-term visiting scholar project (Grant No. 180608DF06) and the China Postdoctoral Science Foundation (2017M622744, 2018T110886); F.G. is a Wallenberg Academy Fellow.

References

1. Shi Z, et al. Transferrable monolithic III-nitride photonic circuit for multifunctional optoelectronics. Appl Phys Lett. 2017; 111
2. Jiang Y, et al. Simultaneous light-emitting light-detecting functionality of InGaN/GaN multiple quantum well diodes. IEEE Electron Device Lett. 2017; 38:1684–1687.
3. Clark J, Lanzani G. Organic photonics for communications. Nat Photonics. 2010; 4:438–446.
4. Klauk, H. Organic electronics: materials, manufacturing and applications. 2006. Organic Electronics: Materials, Manufacturing and Applications
5. Muccini M. A bright future for organic field-effect transistors. Nat Mater. 2006; 5:605–613. [PubMed: 16880804]
6. Shirasaki Y, Supran GJ, Bawendi MG, Bulović V. Emergence of colloidal quantum-dot light-emitting technologies. Nature Photonics. 2013; 7:13–23.
7. García De Arquer FP, Armin A, Meredith P, Sargent EH. Solution-processed semiconductors for next-generation photodetectors. Nature Reviews Materials. 2017; 2
8. Zhang G, et al. Highly efficient photovoltaic diode based organic ultraviolet photodetector and the strong electroluminescence resulting from pure exciplex emission. Org Electron physics Mater Appl. 2009; 10:352–356.
9. Ali F, Periasamy N, Patankar MP, Narasimhan KL. Integrated organic blue LED and visible-blind UV photodetector. J Phys Chem C. 2011; 115:2462–2469.
10. Yoshino K, et al. Marked enhancement of photoconductivity and quenching of luminescence in poly(2,5-dialkoxy-p-phenylene vinylene) upon c60 doping. Jpn J Appl Phys. 1993; 32:L357–L360.
11. Mashford BS, et al. High-efficiency quantum-dot light-emitting devices with enhanced charge injection. Nat Photonics. 2013; 7:407–412.
12. Dai X, et al. Solution-processed, high-performance light-emitting diodes based on quantum dots. Nature. 2014; 515:96–99. [PubMed: 25363773]
13. Oh N, et al. Double-heterojunction nanorod light-responsive LEDs for display applications. Science. 2017; 355:616–619. [PubMed: 28183975]
14. Oertel DC, Bawendi MG, Arango AC, Bulović V. Photodetectors based on treated CdSe quantum-dot films. Appl Phys Lett. 2005; 87

15. Clifford JP, et al. Fast, sensitive and spectrally tuneable colloidal-quantum-dot photodetectors. Nat Nanotechnol. 2009; 4:40–44. [PubMed: 19119281]
16. Tan ZK, et al. Bright light-emitting diodes based on organometal halide perovskite. Nat Nanotechnol. 2014; 9:687–692. [PubMed: 25086602]
17. Sutherland BR, Sargent EH. Perovskite photonic sources. Nature Photonics. 2016; 10:295–302.
18. Dou L, et al. Solution-processed hybrid perovskite photodetectors with high detectivity. Nat Commun. 2014; 5
19. Feng J, et al. Single-crystalline layered metal-halide perovskite nanowires for ultrasensitive photodetectors. Nat Electron. 2018; 1:404–410.
20. Fang Y, Huang J. Resolving weak light of sub-picowatt per square centimeter by hybrid perovskite photodetectors enabled by noise reduction. Adv Mater. 2015; 27:2804–2810. [PubMed: 25786908]
21. Shen L, et al. A Self- Powered, Sub- nanosecond- Response Solution- Processed Hybrid Perovskite Photodetector for Time- Resolved Photoluminescence- Lifetime Detection. Adv Mater. 2016; 28:10794–10800. [PubMed: 27783439]
22. Bao C, et al. Low-noise and large-linear-dynamic-range photodetectors based on hybrid-perovskite thin-single-crystals. Adv Mater. 2017; 29
23. Bao C, et al. High performance and stable all-inorganic metal halide perovskite-based photodetectors for optical communication applications. Adv Mater. 2018; 30
24. Wang N, et al. Perovskite light-emitting diodes based on solution-processed self-organized multiple quantum wells. Nat Photonics. 2016; 10:699–704.
25. Chiba T, et al. Anion-exchange red perovskite quantum dots with ammonium iodine salts for highly efficient light-emitting devices. Nat Photonics. 2018; 12:681–687.
26. Zhao B, et al. High-efficiency perovskite–polymer bulk heterostructure light-emitting diodes. Nat Photonics. 2018; 12:783–789.
27. Cao Y, et al. Perovskite light-emitting diodes based on spontaneously formed submicrometre-scale structures. Nature. 2018; 562:249–253. [PubMed: 30305742]
28. Lin K, et al. Perovskite light-emitting diodes with external quantum efficiency exceeding 20 per cent. Nature. 2018; 562:245–248. [PubMed: 30305741]
29. Xu W, et al. Rational molecular passivation for high-performance perovskite light-emitting diodes. Nat Photonics. 2019; 13:418–424.
30. Deschler F, et al. High photoluminescence efficiency and optically pumped lasing in solution-processed mixed halide perovskite semiconductors. J Phys Chem Lett. 2014; 5:1421–1426. [PubMed: 26269988]
31. Xing G, et al. Low-temperature solution-processed wavelength-tunable perovskites for lasing. Nat Mater. 2014; 13:476–480. [PubMed: 24633346]
32. Stranks SD, et al. Electron-hole diffusion lengths exceeding 1 micrometer in an organometal trihalide perovskite absorber. Science. 2013; 342:341–344. [PubMed: 24136964]
33. Van Le Q, Jang HW, Kim S-Y. Recent advances toward high-efficiency halide perovskite light emitting diodes: review and perspective. Small Methods. 2018; 2
34. Yuan M, et al. Perovskite energy funnels for efficient light-emitting diodes. Nat Nanotechnol. 2016; 11:872–877. [PubMed: 27347835]
35. Wei M, et al. Ultrafast narrowband exciton routing within layered perovskite nanoplatelets enables low-loss luminescent solar concentrators. Nat Energy. 2019; 4:197–205.
36. Liao CL, Chang YF, Ho CL, Wu MC. High-speed GaN-based blue light-emitting diodes with gallium-doped ZnO current spreading layer. IEEE Electron Device Lett. 2013; 34:611–613.
37. Liao CL, Ho CL, Chang YF, Wu CH, Wu MC. High-speed light-emitting diodes emitting at 500 nm with 463-Mhz modulation bandwidth. IEEE Electron Device Lett. 2014; 35:563–565.
38. Kim JS, Kajii H, Ohmori Y. Characteristics of optical response in red organic light-emitting diodes using two dopant system for application to the optical link devices. Thin Solid Films. 2006; 499:343–348.
39. Barlow IA, Kreouzis T, Lidzey DG. High-speed electroluminescence modulation of a conjugated-polymer light emitting diode. Appl Phys Lett. 2009; 94

40. Bowring AR, Bertoluzzi L, O'Regan BC, McGehee MD. Reverse bias behavior of halide perovskite solar cells. Adv Energy Mater. 2018; 8
41. Lochner CM, Khan Y, Pierre A, Arias AC. All-organic optoelectronic sensor for pulse oximetry. Nat Commun. 2014; 5
42. Gong S, et al. A wearable and highly sensitive pressure sensor with ultrathin gold nanowires. Nat Commun. 2014; 5
43. Yokota N, Nisaka K, Yasaka H, Ikeda K. Spin polarization modulation for high-speed vertical-cavity surface-emitting lasers. Appl Phys Lett. 2018; 113
44. Ferreira RXG, et al. High bandwidth GaN-based micro-LEDs for multi-Gb/s visible light communications. IEEE Photonics Technol Lett. 2016; 28:2023–2026.
45. Shimizu N, Watanabe N, Furuta T, Ishibashi T. InP-InGaAs uni-traveling-carrier photodiode with improved 3-dB bandwidth of over 150 GHz. IEEE Photonics Technol Lett. 1998; 10:412–414.

Europe PMC Funders Author Manuscripts

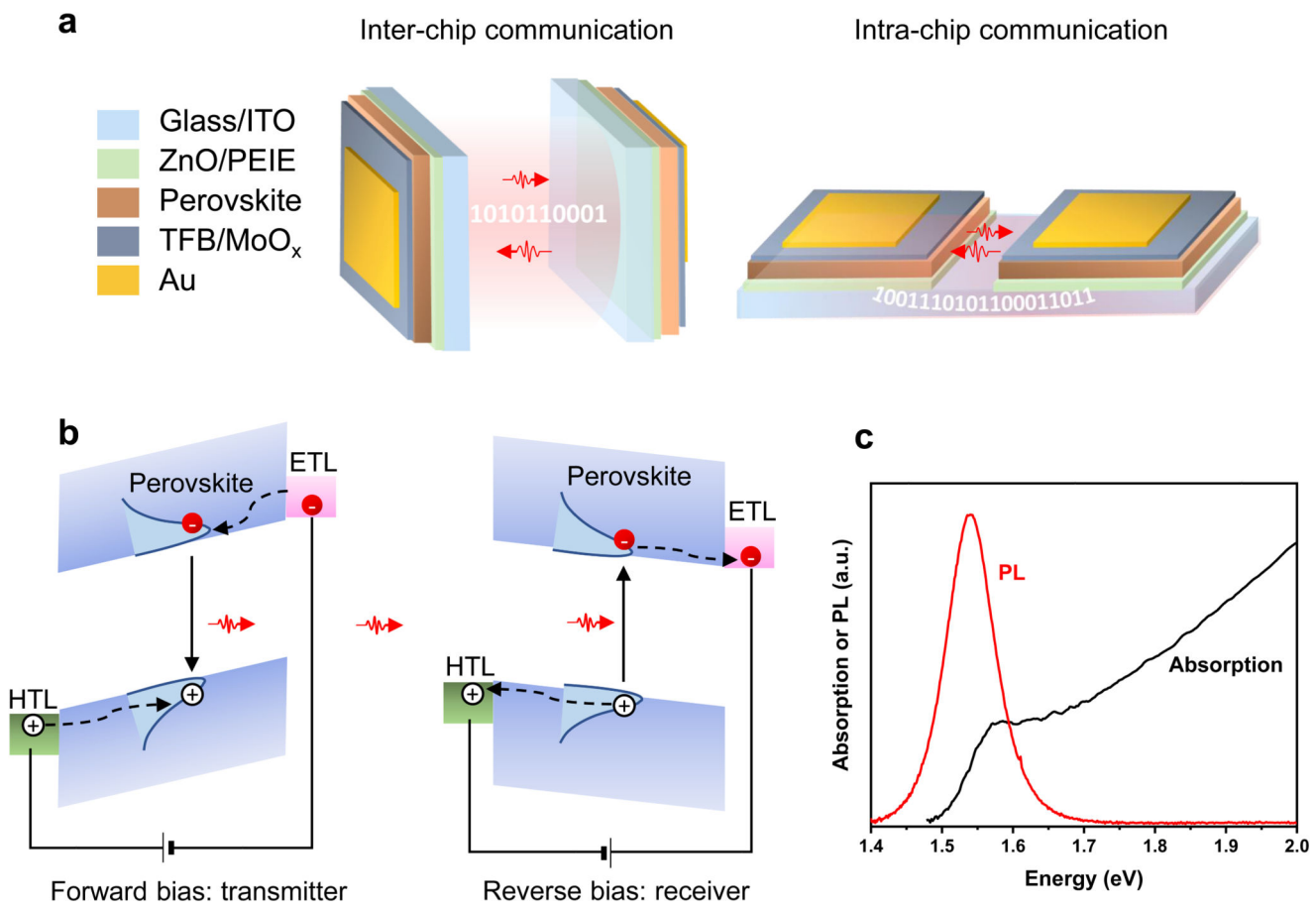

Figure 1. Schematic illustration of the dual-functional perovskite diode used as the light-emitting and detecting devices.

a, schematics of using perovskite diodes for inter- and intra-chip data communications. **b,** Schematics of the energy diagram of the perovskite diode under forward bias as an LED and reverse bias as a photodetector. Light emitted from the forward-biased diode induces photocurrent in the reverse-biased diode. **c,** Absorption and photoluminescence (PL) spectra of the perovskite film. The large spectral overlap enables efficient absorption of the light emitted from the other identical device.

Europe PMC Funders Author Manuscripts

Europe PMC Funders Author Manuscripts

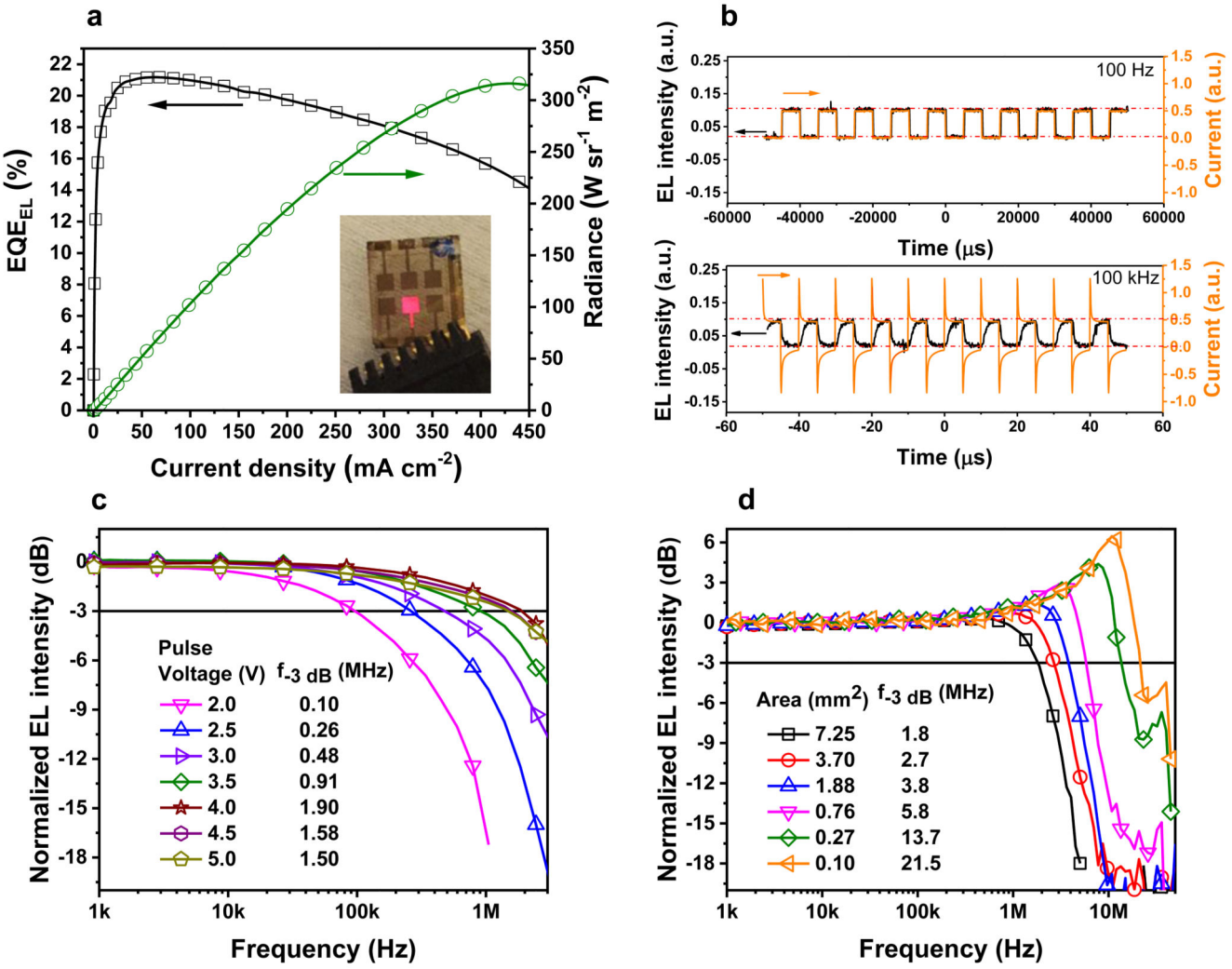

Figure 2. Characterizations of the perovskite diodes when working as the light emitter.

a, External quantum efficiency (EQE) and radiance versus current density curves of the optimized perovskite LEDs. The inset is the photograph of the LED driven by a 3.0 V bias. **b,** Transient EL intensity and current characterization of the perovskite LEDs. **c,** Frequency response curves of the perovskite LED under different drive pulse voltages. **d,** Frequency response of perovskite LEDs with different device areas.

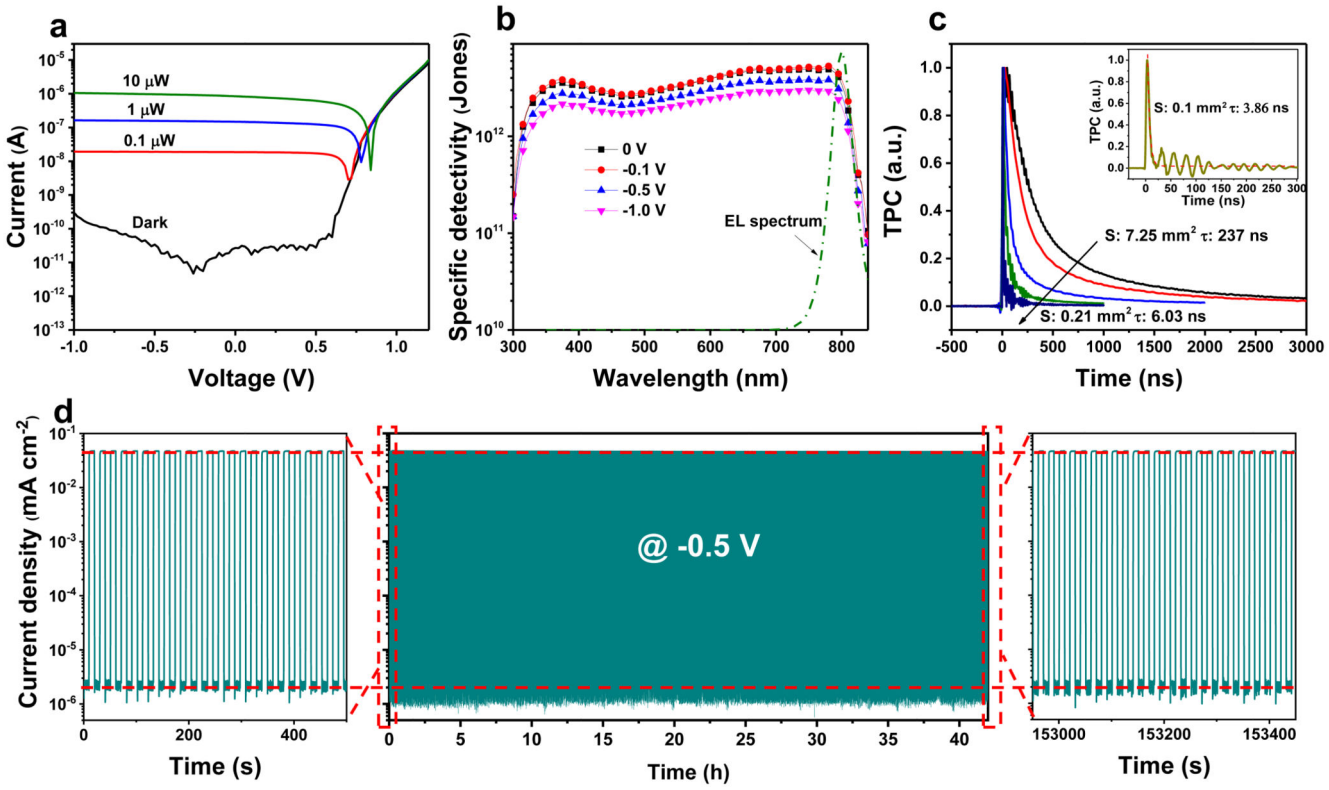

Figure 3. Characterizations of the perovskite diode when working as a photodetector.

a, Current-voltage (I-V) curves of the perovskite photodetector under dark and illuminated light (with different light powers). b**,** Specific detectivity of the perovskite photodetector under different reverse biases, and the electroluminescence **(EL)** spectrum of the same perovskite diode under forward bias. **c,** Transient photocurrent (TPC) characteristics at 0 V bias of perovskite photodetectors with different device areas. **d,** Continuous track of the photo and dark current of the perovskite photodetector under -0.5 V bias during a period of over 42 hours.

Europe PMC Funders Author Manuscripts

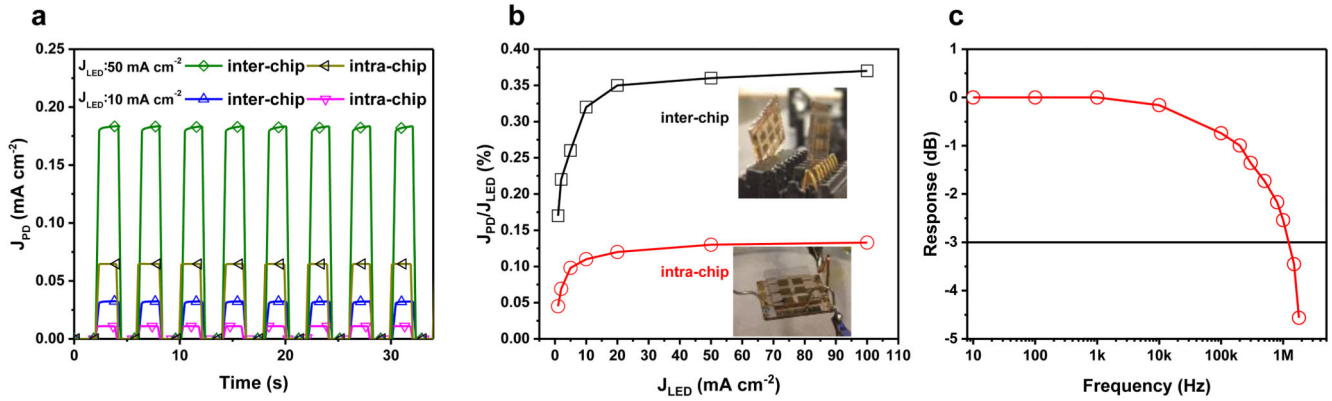

Figure 4. Photoresponse characteristics of the perovskite diode working as a photodetector to light emitted from another identical diode which works as an LED.

a, Photocurrent density of the -0.5 V biased perovskite diode working as a photodetector (J_{PD}), responding to light emitted from an identical perovskite diode working as an LED driven with different current densities (J_{LED}). **b,** The current to current ratios (J_{PD}/J_{LED}) of the -0.5 V biased perovskite photodetector and LED at different LED drive current densities. **c,** Frequency response of the perovskite photodetector to the light emitted from the perovskite LED.

Europe PMC Funders Author Manuscripts

Europe PMC Funders Author Manuscripts

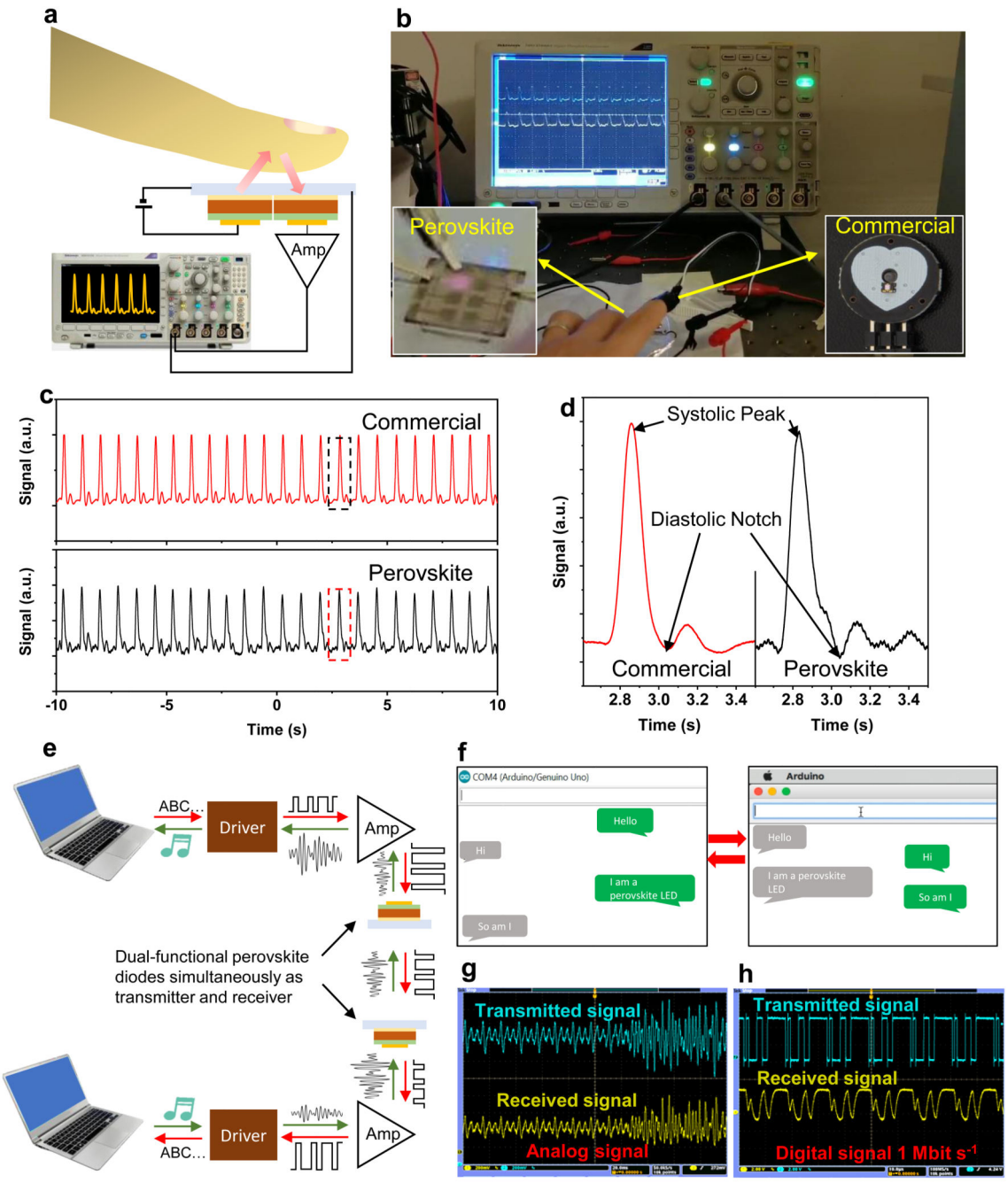

Figure 5. Demonstration of the dual-functional perovskite diode for applications in biomedicine and optical communications.

a, b, Schematic illustration (a) and the photograph (b) of the application of integrated perovskite light source and detector in one chip to be used in heart pulse monitor. **c,** The waveforms of the heart pulse obtained using the commercial and perovskite sensors. **d,** The enlarged waveform of the heart pulse monitored using the commercial and perovskite sensors, which can clearly show the systolic peak and diastolic notch of the pulse signal. **e,** Schematic illustration of using the dual-functional perovskite diode as the transmitter and

receiver in a bidirectional communication system for analogue and digital signals. **f,** The photograph of the user interface of the bidirectional optical communication system using dual-functional perovskite diodes as the transmitter and receiver. The chat bubbles were later-added to guide the eye. **g,** Waveforms of transmitted and received audio analogue signals in the optical communication demonstration system with two inter-chip dual-functional perovskite diodes as the transmitter and receiver. **h,** Waveforms of transmitted and received digital signals between these two dual-functional perovskite diodes at bit rates of 1 Mbit/s.

Europe PMC Funders Author Manuscripts